AD-A059 515 ATLANTIC RESEARCH CORP GAINESVILLE VA F/G 20/4
CALIBRATION PROCEDURES DEVELOPED FOR A TRIAXIAL HOT-FILM PROBE --ETC(U)
MAY 78 L W HARDIN, W H HALL F44620-76-C-0055

UNCLASSIFIED NCSU/EDC-78-4 AFOSR-TR-78-1362 NL

| OF |
AD
A059515

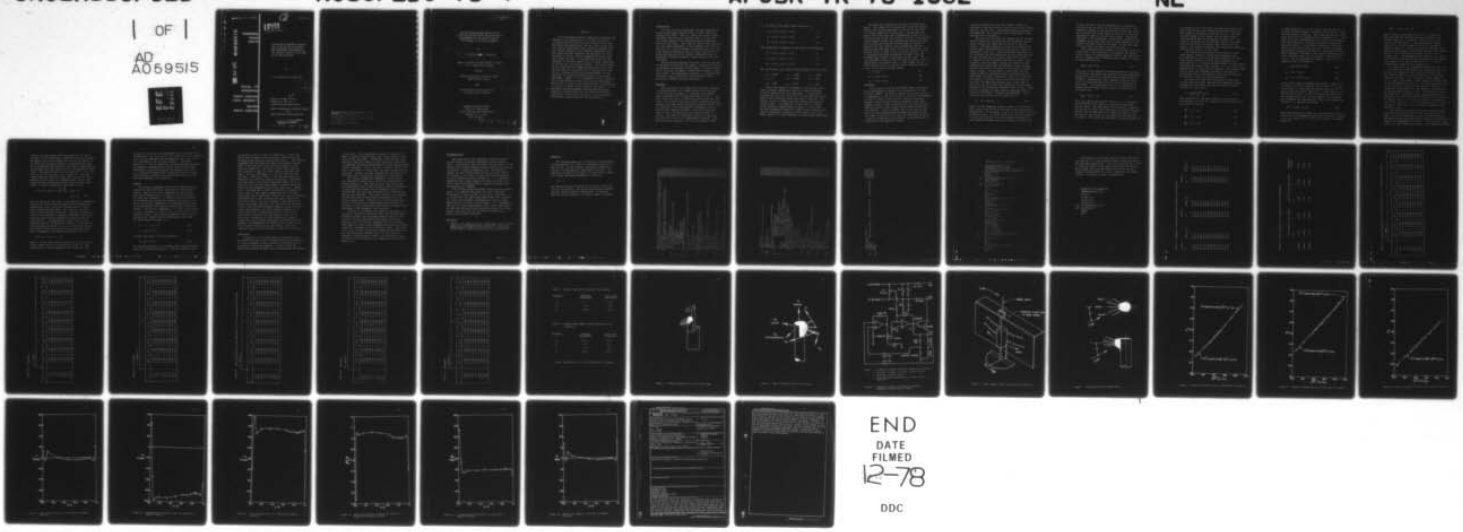

END
DATE
FILMED
12-78
DDC

ENGINEERING
DESIGN
CENTER

SCHOOL OF
ENGINEERING

NORTH CAROLINA
STATE UNIVERSITY

RALEIGH
NORTH CAROLINA

EDC-78-4

LEVEL II

CALIBRATION PROCEDURES DEVELOPED FOR A TRIAXIAL HOT-FILM PROBE AND PRELIMINARY MEASUREMENTS OF THE VELOCITY PROFILE IN THE WAKE OF AN ISOLATED ROTOR

by

L. W. Hardin and W. Hugh Hall

Report on AFOSR Contract
F44620-76-C-0055 for a
cooperative program between

UNITED TECHNOLOGIES RESEARCH CENTER
and
NORTH CAROLINA STATE UNIVERSITY

AIR FORCE OFFICE OF SCIENTIFIC RESEARCH (AFSC)
NOTICE OF TRANSMITTAL TO DDC
This technical report has been reviewed and is approved for public release IAW AFR 190-12 (7b).
Distribution is unlimited.
A. D. BLOSE
Technical Information Officer

(14) NCSU/EDC-78-4

(6)

CALIBRATION PROCEDURES DEVELOPED FOR A TRIAXIAL HOT-FILM PROBE AND PRELIMINARY MEASUREMENTS OF THE VELOCITY PROFILE IN THE WAKE OF AN ISOLATED ROTOR

(9) Interim rept.

by

(10) L. W. Hardin and W. Hugh Hall

(11) 15 May 78

(12) 42p.

(15) Report on AFOSR Contract F44620-76-C-0055
for a cooperative program

(16) 2307

(17) A4

between

United Technologies Research Center
East Hartford, Conn.

(18) AFOSR

and

North Carolina State University
Raleigh, North Carolina

(19) TR-78-1362

Engineering Design Center
School of Engineering
North Carolina State University
Raleigh, N. C. 27650

May 15, 1978

Abstract

In an experiment which was conducted to determine the response of an isolated rotor to an inlet distortion, a triaxial hot-film probe was used to make velocity and flow angle measurements near the exit plane of the rotor. The velocity sensors were three mutually orthogonal film-type sensors operated in the constant temperature mode. This probe has been calibrated and procedures have been developed to extract velocity components from the anemometer output voltages. It has been determined that the proximity of the probe shaft results in severe distortion of the flow over the velocity sensors. The process which has been developed for computing velocities yields satisfactory results in test cases and is expected to be suitable for reducing the data from limited number of flow conditions for which the probe was used in the present experiment. However, it is considered to be too involved and too susceptible to error to be used in experiments where there is either a vast amount of data to be processed or there is no means of spot-checking the results. It is therefore considered mandatory that an improved probe geometry be devised which does not exhibit the degree of interference observed with the probe in question before undertaking to make extensive wake measurements.

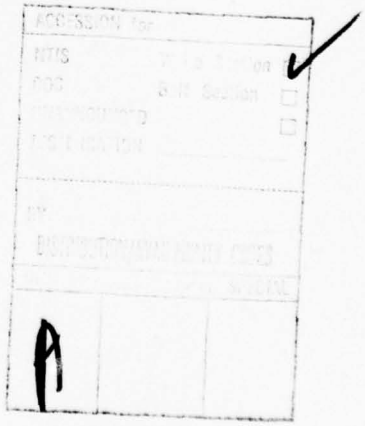

Introduction

An inlet distortion experiment has been conducted in United Technologies Research Center's (UTRC) Large Scale Rotating Rig (LSRR). (Ref. 1) During the course of this experiment some runs were conducted with a triaxial hot-film probe mounted in the rotating reference frame near the rotor exit plane. This probe was used to make velocity and flow angle measurements in the unsteady flow field of the rotor as it passed through a distorted inlet flow. The three mutually orthogonal velocity sensors mounted on the probe were operated in the constant temperature mode by anemometer circuits developed in-house especially for this experiment.

Before the data obtained from such a probe may be used to determine velocity and flow angles, it must be calibrated to determine the response of each sensor to normal velocity and to ascertain the manner in which they respond to transverse flows. The measurements necessary to accomplish this calibration were carried out in North Carolina State University's (NCSU) low speed wind tunnel.

Equipment

The probe used in the LSRR inlet distortion experiment is a Thermo-Systems, Inc. 1296M triaxial hot-film probe. A total pressure transducer is attached to the support shaft resulting in the configuration shown in Fig. 1. Two axes systems are used in calibrating the triaxial hot-film probe. One system is the axial-radial-circumferential axis system of the rotor while the other is chosen with the three axes parallel to the three mutually orthogonal velocity sensors which make up the probe. These two systems are shown in Fig. 2 omitting the total pressure probe for clarity. The velocity components in the two systems may be related by two sets of transformation equations. The first set gives velocities in the rotor reference frame,

v_i, in terms of the sensor frame velocities, u_i.

$$v_1 = a_{11}u_1 + a_{21}u_2 + a_{31}u_3 \quad (1)$$

$$v_2 = a_{12}u_1 + a_{22}u_2 + a_{32}u_3 \quad (2)$$

$$v_3 + a_{13}u_1 + a_{23}u_2 + a_{33}u_3 \quad (3)$$

The second set of equations is the reverse transformation.

$$u_1 = a_{11}v_1 + a_{12}v_2 + a_{13}v_3 \quad (4)$$

$$u_2 + a_{21}v_1 + a_{22}v_2 + a_{23}v_3 \quad (5)$$

$$u_3 = a_{31}v_1 + a_{32}v_2 + a_{33}v_3 \quad (6)$$

The coefficients, a_{ij}, used in these equations are as follows.

$$a_{11} = \sqrt{2/3} \qquad a_{21} = -\sqrt{1/6} \qquad a_{31} = -\sqrt{1/6}$$

$$a_{12} = 0 \qquad a_{22} = -\sqrt{1/2} \qquad a_{32} = \sqrt{1/2}$$

$$a_{13} = \sqrt{1/3} \qquad a_{23} = \sqrt{1/3} \qquad a_{33} = \sqrt{1/3}$$

Each of the sensors is operated in the constant resistance (constant temperature) mode by a circuit developed in-house especially for this experiment. A commercially produced unit was first tried but it failed under the centrifugal loads encountered during operation of the LSRR. The present circuit is compact and quite durable when encapsulated in epoxy. The simplicity of the ciruit is evident in the schematic diagram shown in Figure 3. This circuit has been subsequently modified to make it more versatile and improve performance slightly but the original circuit, as shown, proved to be quite adequate for the present application.

The probe was calibrated in the NCSU Low Speed Wind Tunnel. This tunnel is of conventional closed loop design with the fan located downstream of the test section which is 32 inches high and 45 inches wide. Turning vanes are used in the corners and flow straightening screens are located up-stream of the test section to provide a uniform flow. A probe support fixture was designed which allows the probe to be pitched and yawed while maintaining the sensors in precisely the same location thus allowing any flow non-uniformities which might still exist to be neglected. This fixture, which is shown in Fig. 4, may be pitched $\pm$ 20° in 5° increments and yawed continuously through a full 360° although angle readout is available for only $\pm$ 90° The sign conventions used for the pitch and yaw angles, θ and ϕ, respectively, are shown in Fig. 5. These angles and the total velocity vector, V, may be used to calculate the velocities in the rotor reference frame.

$$v_1 = V \sin \theta \tag{7}$$

$$v_2 = V \cos \theta \sin \phi \tag{8}$$

$$v_3 = V \cos \theta \cos \phi \tag{9}$$

Procedure

The velocity in the Low Speed Wind Tunnel is measured by a slant manometer connected to a pressure port in the settling chamber. The static pressure in the test section is atmospheric as the test section is vented to the atmosphere. In order to obtain a more accurate velocity measurement, a pneumatic total pressure probe was mounted in the probe support fixture so that its head was in the exact position that the sensors of the triaxial probe would occupy when it was inserted. A static pressure port in the test section floor was also monitored and the tunnel was operated over the range of velocities to be used in calibration to obtain a precise calibration of the velocity at the probe head as a function of the manometer reading.

The yawing mechanism of the probe support fixture was adjusted to read zero with the total pressure probe aligned directly into the flow. The pitching mechanism needed no adjustment but this could have been accomplished by shimming the base if necessary.

The total pressure probe was removed and the triaxial hot-film probe was installed into the calibration fixture using a flag on the probe shaft to align it with the fixture. The probe geometry was used to calculate pitch and yaw angles which would place each sensor in turn perpendicular to the flow. Based on previous experience, it was suspected that the probe shaft was deflecting the flow so that the flow was not actually normal to the sensor in question at the calculated pitch and yaw angle. Consequently, with the tunnel running, the probe was yawed slightly while monitoring the anemometer output voltage. The flow was taken to be normal to the sensor at maximum output voltage. The yaw angle at peak output did vary slightly from the calculated values confirming that the probe shaft was indeed interfering with the airflow over the sensors. With each sensor in turn placed normal to the flow, the tunnel was operated over a wide range of velocities and the various flow properties and the output voltage of the appropriate anemometer were recorded. These data are presented in Table I and are plotted in Figs. 6 through 8 for sensors 1 through 3, respectively. It was desired to fit the data to the form of Eq. 10

$$E^2 - E_0^2 = K\sqrt{\rho V}\,(T_s - T_\infty) \quad , \tag{10}$$

where E is the anemometer output voltage, ρ is the density, and T_s and T_∞ are the sensor and free stream temperatures, respectively. The constants E_o and K are determined from the calibration data. No single value of E_o and K was found to be valid over the entire velocity range; consequently, a least squares procedure was used to obtain two curve fits

of the form of Eq. 10, one of which was for the higher velocities and the other, for the lower velocities. The anemometer voltage at the intersection of these two curves was calculated and, along with the values of E_o and K, is presented in Table II for the three sensors. During the remainder of the calibration, if the output voltage of the anemometer was greater than the crossover voltage for that channel, the upper curve fit was used. On the other hand, if it was lower, the lower curve fit was used.

After determining the response of the probe sensors to normal flow, it was necessary to investigate the behavior of the sensors in non-perpendicular flows. One expression which is commonly used to describe the response of a sensor to transverse flow is:

$$q_{eff}^2 = u_n^2 + K^2 u_t^2 \quad , \tag{11}$$

where q_{eff} is the effective velocity measured by the sensor, u_n and u_t are the normal and transverse velocity components, respectively, and K is a constant which is empirically determined. Unfortunately, this expression does not lend itself to situations where the flow may be blocked by the probe shaft. The formulation of Eq. 12 was developed to include these blockage effects as well as sensitivity to transverse flow.

$$q_{eff}^2 = u_n^2 \, f(\theta, \phi) \quad , \tag{12}$$

where q_{eff} and u_n are as before and $f(\theta, \phi)$ is a weighting factor of order unity which is a function of the pitch and yaw angles. The wind tunnel was operated at a constant velocity of 116 ft/sec while the probe was pitched and yawed and the data obtained used to calculate the value of this function for each sensor at each combination of pitch and yaw angles. The values thus obtained are listed in Table III.

For sensors 2 and 3, the values are generally greater than unity with the low values occurring only where the probe shaft might be expected to block the flow (i.e. the flow is nearly normal to the sensor) and the higher values occurring where there is significant traverse flow. For sensor 1, evaluation of the function yielded values much less than unity over the entire range of pitch and yaw angles. This behavior indicates that something is blocking the flow over sensor 1 at all times.

The values of the function at each value of θ were least square fitted to a fifth order polynomial in ϕ. The coefficients of each term in this polynomial were then least squares fitted to a fifth order polynomial in θ resulting in a 5 x 5 matrix of coefficients for each sensor from which the value of the function, $f(\theta, \phi)$, at any intermediate value of θ and ϕ may be computed. The computer codes used to reduce the tabulated function to the matrix of coefficients and to subsequently reconstruct the function at arbitrary θ and ϕ are given in Appendix A.

In order to use the calibration data to obtain the velocity and flow angles from the three anemometer output voltages, one first must calculate an effective normal velocity for each wire by

$$q = \left[\frac{E^2 - E_0^2}{k\sqrt{\rho}\ (T_s - T_\infty)}\right]^2 , \qquad (13)$$

where quantities on the right hand side of the equation are the same as for Eq. 10. Equation 12 may be written for each sensor as follows.

$$\frac{q_1}{f_1}^2 = u_2^2 + u_3^2 \qquad (14)$$

$$\frac{q_2}{f_2}^2 = u_1^2 + u_3^2 \qquad (15)$$

$$\frac{q_3}{f_3}^2 = u_1^2 + u_2^2 \qquad (16)$$

In these equations, f_i is the value of the function $f(\theta, \phi)$ for the ith sensor which is evaluated at the value of θ and ϕ from the previous iteration. These equations may be solved quite easily for the squared velocity components, u_i^2. Since there is no way to know whether u_i is positive or negative from these equations, the proper sign must be known from some other source. In the present experiment, the orientation of the probe was such that the velocity components may always be assumed to be positive. Using the transformation equations 1 through 3, the velocity components in the rotor reference frame, v_i, are computed. The total velocity, V, and the resultant flow angles, θ_r and ϕ_r, are calculated by Eqs. 17 through 19.

$$V = \sqrt{v_1^2 + v_2^2 + v_3^2} \tag{17}$$

$$\theta_r = \sin^{-1}(v_1/V) \tag{18}$$

$$\phi_r = \sin^{-1}(v^2/V \cos \theta) \tag{19}$$

In all cases tested, the method overcorrects. That is, if the value of ϕ used to evaluate the functions $f(\theta, \phi)$ is correct but θ is lower than the correct value, θ_r will be greater than the correct value of θ. If the value of θ is not greatly in error, ϕ_r will be essentially the same as the assumed value of ϕ. For this reason, the iterations were uncoupled and under-relaxed. Thus, with θ being held constant, ϕ is iterated upon using

$$\phi^{n+1} = 0.8\phi^n + 0.2\phi_r{}^n \tag{20}$$

where the superscripts denote the iteration level. When ϕ^n and $\phi_r{}^n$ have converged within the desired tolerence (normally 2.5°), the value of ϕ^{n+1} is set by Eq. 20 and θ is updated by Eq. 21.

$$\theta^{n+1} = 0.8\ \theta^{n} + 0.2\ \theta_r^{n} \quad . \tag{21}$$

When θ has also converged, the process is terminated. Note that when the iteration has been terminated, the correct value of θ is between θ^n and θ_r^n which are in error by the tolerence, ε. Thus choosing the computed value of θ to be the average of θ^n and θ_r^n guarantees accuracy within $\varepsilon/2$. However, due to the overshoot which appears to be inherent in the method, allowing the computed value of θ to be defined by equation 21 gives a lower average error. (The maximum possible error for any single calculation is 0.8ε when using this method but the average error appears to be on the order of 0.2ε.) A similar argument may be made for the evaluation of ϕ.

As a test case, the anemometer voltages obtained from a run in which the rotor blades were removed and the rotor was run very slowly in order to survey the flow field, were inserted into Eq. 13 and the process previously outlined was followed. Here, all three velocity components, v_1, v_2, and v_3, were known. There should be no radial flow, v_1, the circumferential velocity, v_2, should be entirely due to the rotation of the rotor, and the axial velocity, v_3, should match that measured by the pneumatic instrumentation in the stationary reference frame. (The pneumatic instrumentation used to measure the axial velocity was normally used only to set the flow condition and is not very accurate. It normally gave an axial velocity somewhat less than the true value. However, it was all that was available in this one case.) All three calculated velocity components were grossly in error.

Since there were previous indications that the probe shaft was interferring with the flow over the sensors and might in fact be generating a region of separated flow, it was theorized that the directional calibration functions $f(\theta, \phi)$ might not be independent of velocity. To verify this supposition, the wind tunnel was operated at the maximum attainable

velocity (to more closely match the velocities in the experiment) and new directional calibration data were obtained. The angles used in this second test are not the same as in the first test because preliminary calculations using the first calibration indicated that ϕ was almost always negative in the higher velocity regions of the flow downstream of the rotor. The values obtained for the function $f(\theta, \phi)$ at this velocity (159 ft/sec) are listed in Table IV. The same trends which were observed at the lower velocity are still apparent but the values are somewhat higher overall indicating that the interference of the probe shaft has diminished. A linear interpolation was applied so that

$$f(\theta, \phi) = f_L(\theta, \phi) + \frac{V - V_L}{V_H - V_L} - [f_H(\theta, \phi) - f_L(\theta, \phi)] \quad (22)$$

where f_L and f_H are the values of the function as determined from the low velocity and the high velocity calibrations, respectively, and V_L and V_H are the velocities at which those calibrations were done. The velocity V was determined from the previous iteration. Using this procedure in the test case resulted in reasonable agreement between the calculated axial and circumferential velocities and the actual values. A strong radially inward flow was still indicated and this was known not to exist. It was observed that increasing the value of $f(\theta, \phi)$ for the first sensor would tend to bring the radial velocity into better agreement; consequently, this function was modified to be

$$\bar{f}_1(\theta, \phi) = f_1(\theta, \phi) + \Delta f$$

where f_1 is the value calculated from Eq. 22, Δf is the increment added, and $\bar{f}_1$ is the value used in Eq. 14. The calculation of velocity components was carried out with

various Δf's until one was found which gave zero radial flow. At this point, the radial and circumferential velocity components were in close agreement with the expected values of v_1 and v_2 as is indicated by the listing in Table V. The axial velocity, v_3, does not match but, as was previously mentioned, the pneumatic instrumentation used to make this particular measurement is not very accurate. The source of the error in f is presently unknown and if there had not been a known flow condition included in the experimental data, it would have been impossible to evaluate it.

Results

The velocity components for the run in which the rotor blades were removed are now a good match to the expected values. However, the radial component was forced to be zero and the method used to accomplish this also affected the other two components. In order to check the validity of the method, the calibration constants were used to calculate the velocity components at various gapwise locations for an undistorted flow condition resulting in light blade loading. The velocity components v_1, v_2, and v_3 are plotted in Figs. 9 through 11, respectively, as a function of their gapwise position. These velocity components may be used to calculate the relative velocity downstream of the rotor, W_2, and the exit flow angle, β_2.

$$W_2 = v_1^2 + v_2^2 + v_3^2 \tag{24}$$

$$\beta_2 = \tan^{-1}(v_3/v_2) \tag{25}$$

A radial flow angle, ψ, may be defined as

$$\psi = \tan^{-1}(v_1/v_3) \tag{26}$$

The relative velocity, W_2, is normalized by its gap averaged value, $\overline{W}_2$, and plotted in Fig. 12. The flow angles β_2 and ψ

are plotted in Figs. 13 and 14, respectively. These parameters were integrated across the gap to obtain their gap-averaged values which are presented in Table VI. The velocity components and flow angles obtained from pneumatic measurements in the stationary frame are also available in this table for comparison. The axial velocity shows extremely good agreement as does the radial velocity and radial flow angle. The exit flow angle, β_2, does not show this good agreement. Referring to Fig. 13, one observes that large fluctuations in exit flow angle are indicated. Admittedly, the probe used in the present experiment should not be expected to yield accurate measurements in regions which have large velocity gradients (such as the blade wake). However, even if the magnitude of these fluctuations is somewhat in error, there is still ample evidence that the flow angle fluctuations are of sufficient intensity to cause the pneumatic instrumentation to give erroneous flow angle indications. Upon this evidence, the use of pneumatic instrumentation to measure flow angles near the rotor exit (both the rotating triaxial probe and the stationary pneumatic wedge probe were located approximately .05 chord lengths downstream of the rotor exit plane) is highly questionable. The overall trends tend to indicate that the correction made to the directional calibration is valid because good agreement between the triaxial probe measurements and those made with pneumatic instrumentation was obtained for the empty tunnel (rotor blades removed) and for the lightly loaded flow condition except for the variations in the exit flow angle, β_2.

Conclusions

Virtually all of the difficulties encountered during the calibration process and in applying the calibration data to convert anemometer output voltages to velocities may be attributed to the probe geometry. It appears that one should avoid having the probe shaft located behind the sensors

at all costs. This limitation may render it impossible to mount a triaxial velocity sensor and a total pressure transducer on the same shaft. Furthermore, the relatively wide spacing of the three sensors on this particular probe leads to erroneous flow angle measurements in regions having strong velocity gradients. One of the areas of prime interest, the flow in the wake of a rotor blade, has these strong velocity gradients. Overall, one must conclude that the geometry of the probe used in the present experiment is rather poor.

The constant temperature anemometer circuits which were designed in-house especially for this experiment performed flawlessly. There was initially some concern that the centrifugal loads to which the units would be subjected in this application might lead to mechanical failure as had been the case with some commercial units which had previously been installed. These fears proved to be unfounded and the units did not even require adjustment after the initial installation. Therefore, it is believed that this circuit is well suited to applications which require the tolerence of high acceleration loads and do not permit easy adjustment of the anemometer once installed.

In spite of the problems introduced by the geometry of the probe, calibration procedures have been developed which accurately measure the directional characteristics of the sensors. For this particular probe, these directional characteristics are velocity dependent and for one sensor they appear to involve some dependence which can not be identified and reproduced in the calibration tunnel. The use of a test case in which the velocity components were known permits the directional characteristics of this sensor as measured in the calibration tunnel to be corrected so that velocities and flow angles may be computed from the experimental data.

Recommendations

The probe used in this experiment required entirely too much effort to achieve meaningful velocity measurements. In particular, the directional characteristics of the sensors were velocity dependent and one sensor gave evidence of being in a region of separated flow. The measuring volume, the space within which the three velocity sensors are located, is too large to permit accurate measurements in flows having high velocity gradients. It is considered imperative that a probe geometry be found which does not entail these difficulties before extensive rotating frame measurements are attempted.

From the flow angle measurements made with the triaxial probe, it is apparent that there are severe flow angle fluctuations in the near wake of the rotor. Therefore, it is certain that flow angle measurements made near the rotor exit plane with pneumatic instrumentation (such as wedge probes) will be in error to some extent. It is recommended that the flow angle measurements in any future experiments be made with hot-wire or hot-film probes so that the instantaneous flow angles may be accurately determined and a proper average angle calculated.

References

1. Hardin, L.W., and F.O. Carta: The Response of an Isolated Rotor to a Low Frequency Inlet Distortion. Report on AFOSR Contract F44620-76-C-0055, EDC-78-1, Engineering Design Center, North Carolina State University (1978).

Appendix A

The following pages are a listing of a program which converts the data in a table to a polynomial curve fit in two varibles. A least squares technique is employed to achieve a certain degree of smoothing of the data. The subroutine referred to as SIMQ is a system library routine for solving simultaneous equations of the form

$$A\ x = B.$$

The solution vector is returned in B and the coefficient vector A is destroyed. Any system routine which performs the same function could be substituted. In the event that one is not available, a listing of SIMQ is included.

```
C   PROGRAM FOR GENERATING LEAST SQUARES FIT TO DIRECTIONAL CALIBRATION 00000010
      DIMENSION F(3,9,9),THETA(20),PHI(20),A(3,9,5),YDUM(20),COEF(20)   00000020
      RTD=57.29578                                                      00000030
C   READ IN F(NWIRE,ITHETA,JPHI) AND THE THETA AND PHI ARRAYS           00000040
      READ(1,900)((THETA(I),PHI(J),(F(N,I,J),N=1,3),J=1,9),I=1,9)       00000050
      DO 100 IJK=1,9                                                    00000060
      THETA(IJK)=THETA(IJK)/RTD                                         00000070
100   PHI(IJK)=PHI(IJK)/RTD                                             00000080
C   THE FOLLOWING SUBSCRIPT NOTATION WILL BE USED                       00000090
C     N   WIRE NUMBER                                                  00000100
C     I   THETA SUBSCRIPT                                              00000110
C     J   PHI SUBSCRIPT                                                00000120
C     KI  K-TH HARMONIC IN THETA                                       00000130
C     KJ  K-TH HARMONIC IN PHI                                         00000140
C   ALL OTHERS ARE DUMMY SUBSCRIPTS                                     00000150
C                                                                       00000160
C   FIT F AS A FUNCTION OF PHI FOR EACH WIRE (N) AND THETA (I)          00000170
      DO 300 N=1,3                                                      00000180
      DO 300 I=1,9                                                      00000190
C   PUT F INTO A DUMMY VECTOR                                           00000200
      DO 200 J=1,9                                                      00000210
200   YDUM(J)=F(N,I,J)                                                  00000220
C   COMPUTE POLYNOMIAL LEAST SQUARES FIT                                00000230
      CALL POLYSQ(PHI,YDUM,COEF,9,5,KRET)                               00000240
C   STORE THESE COEFFICIENTS                                            00000250
      DO 300 KJ=1,5                                                     00000260
300   A(N,I,KJ)=COEF(KJ)                                                00000270
C   CURVE FIT THESE COEFFICIENTS AS FUNCTIONS OF THETA                  00000280
      DO 500 N=1,3                                                      00000290
      DO 500 KJ=1,5                                                     00000300
      DO 400 I=1,9                                                      00000310
400   YDUM(I)=A(N,I,KJ)                                                 00000320
      CALL POLYSQ(THETA,YDUM,COEF,9,5,KRET)                             00000330
C   STORE FIT                                                           00000340
      DO 500 KI=1,5                                                     00000350
500   A(N,KI,KJ)=COEF(KI)                                               00000360
C   COEFFICIENTS ARE NOW CALCULATED... WRITE INTO DATASET.              00000370
```

```
      DO 600 N=1,3                                                    00000380
600   WRITE(4,901)((A(N,I,J),J=1,5),N,I,I=1,5)                        00000390
      STOP                                                            00000400
900   FORMAT(5F13.7)                                                  00000410
901   FORMAT(5E14.7,2I5)                                              00000420
      END                                                             00000430
      SUBROUTINE POLYSQ(X,Y,B,NPTS,NTERMS,KRET)                       00000440
C   POLYNOMIAL LEAST SQUARES FIT                                      00000450
C     X           INDEPENDENT VARIABLE                              00000460
C     Y           DEPENDENT VARIABLE                                00000470
C     B           COEFFICIENT VECTOR FOR POLYNOMIAL                 00000480
C     NPTS        NUMBER OF POINTS TO BE FIT                        00000490
C     NTERMS      NUMBER OF TERMS TO BE IN POLYNOMIAL               00000500
C     KRET        0 INDICATES GOOD FIT...1 INDICATES FIT FAILED     00000510
      DIMENSION X(20),Y(20),B(20),A(20,20)                            00000520
C   CHECK FOR AN APPROPRIATE ORDER OF EQUATION                        00000530
      IF(NTERMS.GE.NPTS)NTERMS=NPTS-1                                 00000540
C   FORM MARTIX OF COEFFICIENTS                                       00000550
      DO 200 I=1,NTERMS                                               00000560
      DO 200 J=1,NTERMS                                               00000570
      IF(I+J.NE.2)GO TO 100                                           00000580
      A(I,J)=FLOAT(NPTS)                                              00000590
      GO TO 200                                                       00000600
100   A(I,J)=0.0                                                      00000610
      IEXP=I+J-2                                                      00000620
      DO 199 K=1,NPTS                                                 00000630
199   A(I,J)=A(I,J)+X(K)**IEXP                                        00000640
200   CONTINUE                                                        00000650
C   FORM VECTOR FOR RIGHT HAND SIDE OF EQUATION                       00000660
      B(1)=0.0                                                        00000670
      DO 300 K=1,NPTS                                                 00000680
300   B(1)=B(1)+Y(K)                                                  00000690
      DO 400 I=2,NTERMS                                               00000700
      B(I)=0.0                                                        00000710
      IEXP=I-1                                                        00000720
      DO 400 K=1,NPTS                                                 00000730
400   B(I)=B(I)+Y(K)*X(K)**IEXP                                       00000740
      CALL SIMQ(A,B,20,NTERMS,KRET)                                   00000750
```

```
      IF(KRET.EQ.0)RETURN                                                    00000760
      WRITE(3,500)                                                           00000770
500   FORMAT(//'  **************    SINGULAR SOLUTION    **************'/)00000780
      RETURN                                                                 00000790
      END                                                                    00000800
END OF DATA
```

```
      SUBROUTINE SIMQ (A,B,ND,N,KS)

      DIMENSION A(ND,ND),B(ND)
      LOGICAL*1 BIGEXF,DIVEXF
      EQUIVALENCE (DIV,DIVEXP),(BIGA,BIGEXF)
      REAL DIV/Z00100000/,TOL/Z3C800000/
      DO 300 I=1,N
      BIGA=0.
      DO 100 J=1,N
100   BIGA=AMAX1(BIGA,ABS(A(I,J)))
      DIVEXP=BIGEXF
      DO 200 J=1,N
200   A(I,J)=A(I,J)/DIV
300   B(I)=B(I)/DIV
      KS=0
      JJ=-N
      DO  9  J=1,N
      JP1=J+1
      BIGA=0.0
      DO  2  I=J,N
      IF(ABS(BIGA)-ABS(A(I,J)))1,2,2
1     BIGA=A(I,J)
      IMAX=I
2     CONTINUE
      IF(ABS(BIGA)-TOL)3,3,4
3     KS=1
      IF(BIGA.EQ.0.)RETURN
4     DO  6  K=J,N
      IF(IMAX-J)5,6,5
5     SAVE=A(IMAX,K)
      A(IMAX,K)=A(J,K)
      A(J,K)=SAVE
6     A(J,K)=A(J,K)/BIGA
      SAVE=B(IMAX)
      B(IMAX)=B(J)
      B(J)=SAVE/BIGA
      IF(J-N)7,10,7
7     DO  9  IX=JP1,N
      DO  8  JX=JP1,N
8     A(IX,JX)=A(IX,JX)-A(IX,J)*A(J,JX)
9     B(IX)=B(IX)-B(J)*A(IX,J)
10    NY=N-1
      DO  11 J=1,NY
      IB=N-J
      IC=N
      DO  11 K=1,J
      B(IB)=B(IB)-A(IB,IC)*B(IC)
11    IC=IC-1
      RETURN
      END
```

The polynomial coefficients may be used to reconstruct the function, f, at any arbitrary value of theta and phi by the algorithm listed below. Since this algorithm will return a result for values of the angles far outside the range of the original data (and this result may well be in error because the polynomial fit is not a good means of extrapolation) , one must be careful in applying it.

```
      FUNCTION FPT(PHI,THETA,N)
      COMMON/DCOF/A(3,5,5)
      FPT=0.0
      DO 200 I=1,5
      C=A(N,5,6-I)
      DO 100 J=2,5
  100 C=C*THETA+A(N,6-J,6-I)
  200 FPT=FPT*PHI+C
      RETURN
      END
```

Table I. Response of the Three Velocity Sensors to Normal Flow.

Sensor 1		Sensor 2		Sensor 3	
E^2	$\sqrt{\rho V}(T_s-T_\infty)$	E^2	$\sqrt{\rho V}(T_s-T_\infty)$	E^2	$\sqrt{\rho V}(T_s-T)$
21.42	127.2	22.97	126.8	19.95	126.8
22.83	141.4	24.51	141.0	21.46	141.0
23.97	152.4	25.72	151.9	22.42	151.9
24.70	158.8	26.11	157.6	23.04	155.4
24.91	161.3	26.71	160.9	23.27	160.9
25.50	164.7	27.04	163.9	23.71	162.7
25.68	168.5	27.65	168.5	23.98	168.0
26.63	175.8	27.98	174.4	24.70	172.2
27.04	179.1	28.62	178.3	25.10	176.9
28.30	188.3	29.49	186.9	25.81	184.7
28.52	190.8	29.81	190.0	26.11	188.3
29.49	197.9	30.58	196.7	26.83	194.5
29.70	200.7	31.14	200.0	27.25	198.2
30.36	205.8	31.92	204.9	27.77	202.8

Table II Least Squares Fits to Normal Velocity Calibration.

	Low Velocity (116 ft/sec)		High Velocity (159 ft/sec)		Crossover Voltage
	E_0^2	K	E_0^2	K	
Sensor 1	8.262	0.1032	5.499	0.1208	4.947
Sensor 2	8.809	0.1115	7.491	0.1182	5.545
Sensor 3	7.744	0.0967	7.660	0.0987	3.436

Table III. Values Obtained for the Function $f(\theta, \phi)$ at a velocity of 116 ft/sec.

a) Sensor 1.

	θ								
φ	20.0	15.0	10.0	5.0	0.0	-5.0	-10.0	-15.0	-20.0
10.0	0.542	0.531	0.530	0.523	0.542	0.528	0.565	0.555	0.572
5.0	0.529	0.518	0.520	0.516	0.527	0.518	0.546	0.548	0.560
0.0	0.521	0.516	0.521	0.507	0.527	0.515	0.563	0.556	0.556
-5.0	0.536	0.533	0.534	0.525	0.539	0.524	0.581	0.557	0.555
-10.0	0.555	0.545	0.551	0.543	0.541	0.541	0.582	0.560	0.562
-15.0	0.582	0.568	0.569	0.552	0.556	0.589	0.581	0.567	0.568
-20.0	0.621	0.592	0.594	0.578	0.570	0.603	0.592	0.576	0.582
-25.0	0.640	0.664	0.650	0.633	0.601	0.616	0.616	0.602	0.595
-30.0	0.724	0.701	0.682	0.654	0.620	0.592	0.604	0.612	0.630

Table III. Continued.

b) Sensor 2.

	θ								
ϕ	20.0	15.0	10.0	5.0	0.0	-5.0	-10.0	-15.0	-20.0
10.0	0.983	1.002	0.998	0.978	1.015	0.988	0.959	0.974	1.022
5.0	1.033	1.036	1.009	0.993	1.019	0.922	0.916	0.918	0.947
0.0	1.088	1.074	1.056	0.066	0.979	0.941	0.938	0.939	0.950
-5.0	1.134	1.142	1.052	1.011	1.005	0.965	0.952	0.927	0.973
-10.0	1.179	1.179	1.080	1.068	1.039	1.017	0.975	0.973	1.007
-15.0	1.210	1.130	1.138	1.114	1.091	1.061	1.025	0.991	1.025
-20.0	1.282	1.207	1.201	1.197	1.168	1.138	1.109	1.036	1.049
-25.0	1.319	1.350	1.291	1.291	1.309	1.218	1.228	1.138	1.087
-30.0	1.393	1.476	1.429	1.424	1.458	1.412	1.407	1.302	1.230

Table III. Concluded.

c) Sensor 3.

	θ								
ϕ	20.0	15.0	10.0	5.0	0.0	-5.0	-10.0	-15.0	-20.0
10.0	1.188	1.060	1.026	0.984	0.997	0.887	0.793	0.731	0.721
5.0	1.119	1.118	0.976	0.939	0.957	0.844	0.794	0.766	0.753
0.0	1.065	1.057	1.004	0.897	0.923	0.826	0.799	0.797	0.784
-5.0	1.027	1.006	0.962	0.937	1.004	0.825	0.829	0.815	0.807
-10.0	0.999	0.000	0.973	0.958	0.974	0.840	0.817	0.804	0.812
-15.0	0.972	0.981	0.976	0.951	0.962	0.863	0.815	0.819	0.829
-20.0	0.981	0.970	0.962	0.958	0.966	0.830	0.837	0.941	0.964
-25.0	0.958	0.947	0.936	0.937	0.996	0.960	0.964	0.982	1.012
-30.0	0.946	0.950	0.950	0.954	1.009	0.975	0.982	0.998	1.035

Table IV. Values Obtained for the Function $f(\theta, \phi)$ at a velocity of 159 ft/sec.

a) Sensor 1.

	θ								
φ	20.0	15.0	10.0	5.0	0.0	-5.0	-10.0	-15.0	-20.0
20.0	0.561	0.481	0.573	0.576	0.588	0.582	0.585	0.582	0.575
15.0	0.524	0.454	0.551	0.566	0.560	0.566	0.566	0.561	0.566
10.0	0.495	0.434	0.527	0.551	0.544	0.546	0.559	0.581	0.555
5.0	0.484	0.433	0.522	0.545	0.536	0.552	0.549	0.584	0.586
0.0	0.490	0.425	0.527	0.535	0.539	0.554	0.551	0.585	0.573
-5.0	0.530	0.447	0.553	0.562	0.566	0.567	0.564	0.599	0.587
-10.0	0.577	0.490	0.574	0.584	0.589	0.590	0.575	0.596	0.599
-15.0	0.617	0.513	0.618	0.616	0.608	0.613	0.597	0.592	0.610
-20.0	0.665	0.576	0.644	0.645	0.640	0.631	0.619	0.615	0.592

Table IV. Continued.

b) Sensor 2.

	θ								
φ	20.0	15.0	10.0	5.0	0.0	-5.0	-10.0	-15.0	-20.0
20.0	0.997	1.012	0.994	0.952	0.968	0.946	0.963	0.979	0.996
15.0	1.009	1.029	1.014	0.981	0.964	0.948	0.951	0.950	0.990
10.0	1.012	1.056	0.988	0.982	0.973	0.941	0.950	0.957	0.957
5.0	1.040	1.094	1.010	1.992	0.971	0.950	0.944	0.936	0.941
0.0	1.076	1.120	1.068	1.039	0.985	0.950	0.933	0.930	0.919
-5.0	1.120	1.182	1.094	1.055	1.013	0.967	0.915	0.923	0.917
-10.0	1.152	1.230	1.131	1.108	1.055	0.976	0.939	0.911	0.912
-15.0	1.189	1.287	1.200	1.147	1.088	1.029	0.959	0.921	0.885
-20.0	1.253	1.379	1.257	1.199	1.165	1.076	1.004	0.912	0.887

Table IV. Concluded.

c) Sensor 3.

	θ								
ϕ	20.0	15.0	10.0	5.0	0.0	-5.0	-10.0	-15.0	-20.0
20.0	1.394	1.520	1.375	1.329	1.280	1.198	1.075	0.962	0.854
15.0	1.307	1.398	1.262	1.223	1.178	1.074	0.989	0.915	0.847
10.0	1.258	1.345	1.197	1.163	1.098	1.029	0.931	0.897	0.867
5.0	1.184	1.245	1.140	1.090	1.061	1.006	0.920	0.899	0.888
0.0	1.118	1.187	1.097	1.060	1.018	0.974	0.951	0.920	0.904
-5.0	1.087	1.117	1.067	1.043	1.015	0.984	0.973	0.937	0.917
-10.0	1.068	1.084	1.026	1.062	1.022	0.983	0.967	0.946	0.945
-15.0	1.059	1.064	1.064	1.045	1.020	0.999	0.974	0.993	0.988
-20.0	1.057	1.054	1.047	1.042	1.057	1.003	0.997	1.011	1.023

Table V. Results from Test with Rotor Blades Removed.

Parameter	Pneumatic Measurement	Triax Probe Measurement
v_1	0	0.13
v_2	-7.27	-8.06
v_3	68.70	76.69

Table VI. Results from Lightly Loaded Undistorted Flow Condition.

Parameter	Pneumatic Measurement	Triax Probe Measurement
W_2	143.5	155.9
β_2	64.2	62.3
ψ	0.0	0.5
C_x	129.0	131.8

Note: Velocities are in ft/sec and angles in degrees.

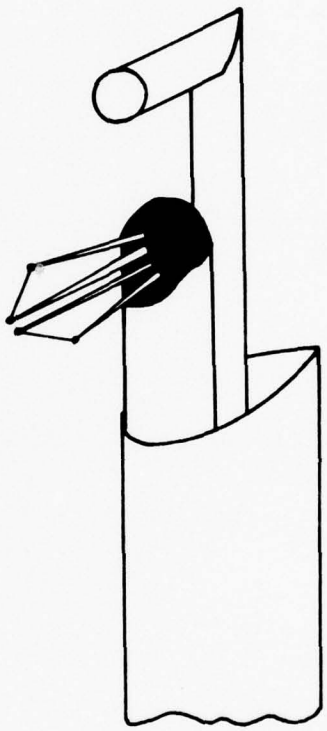

Figure 1. Overall Configuration of the Wake Probe.

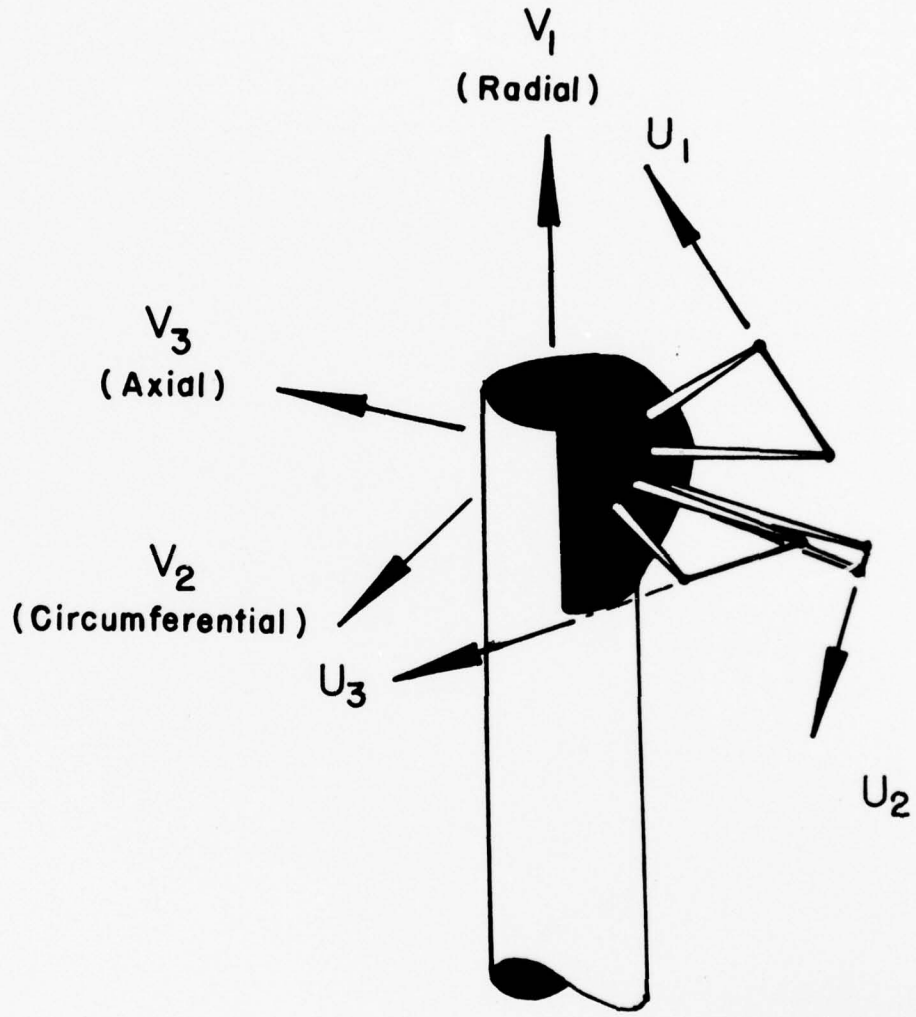

Figure 2. Rotor and Sensor-based Axis Systems.

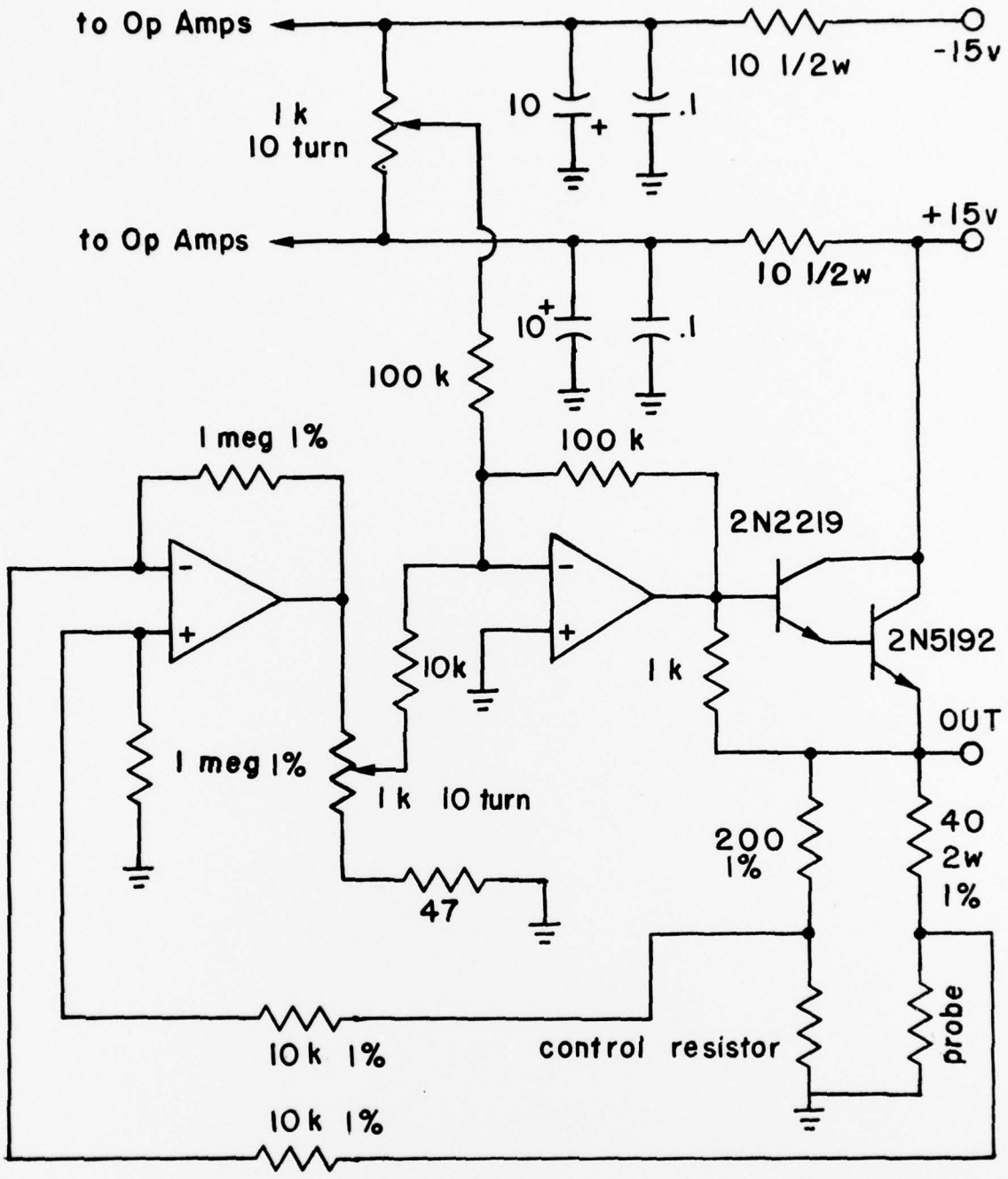

NOTES:
1. Op Amps are LM301A with 30pf compensation capacitor.
2. Resistors in ohms. 1/4 watt 5% unless noted.
3. Capacitors in microfarads.
4. Probe operating resistance is 5 times control resistor.

Figure 3. Schematic Diagram of Constant Temperature Anemometer Circuit Used in LSRR.

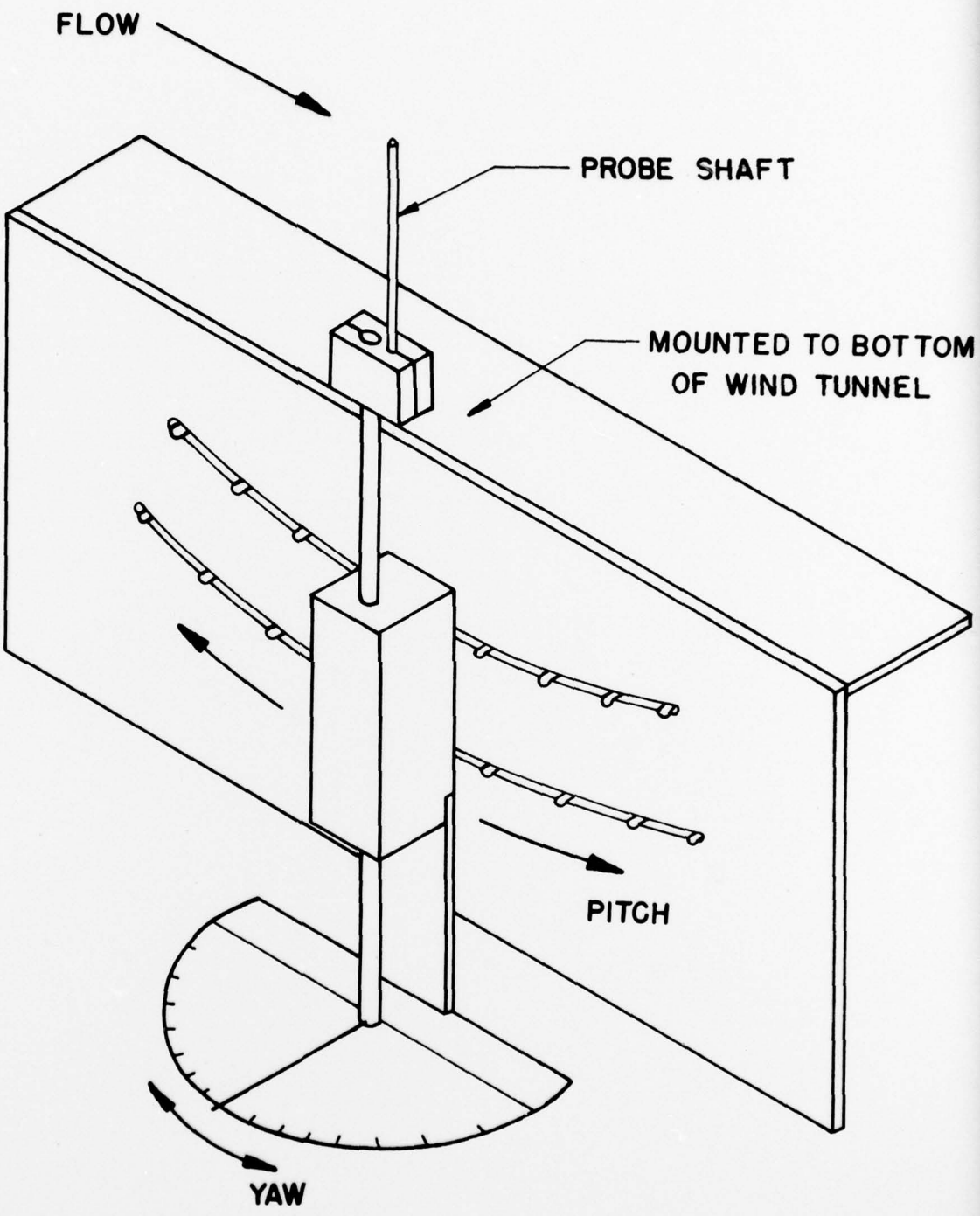

Figure 4. Probe Support Fixture Used During Calibration.

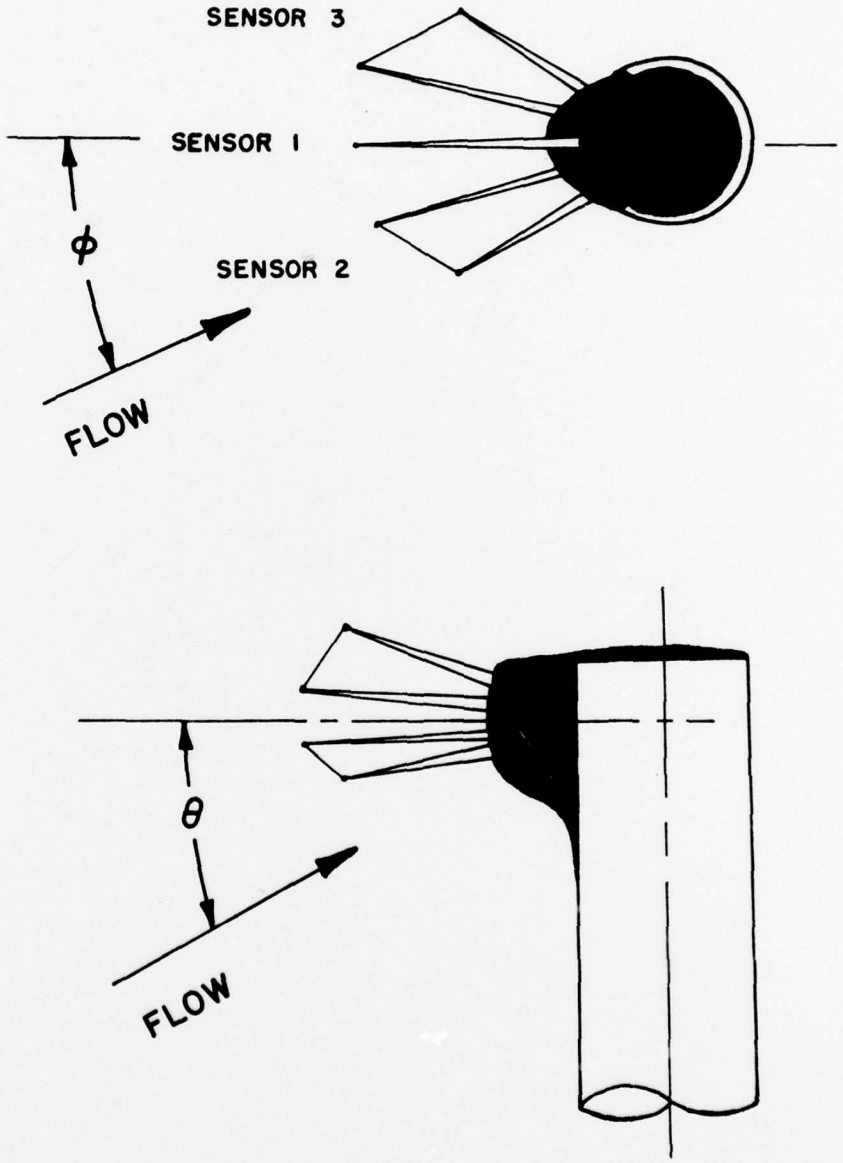

Figure . Pitch and Yaw Angle Nomenclature.

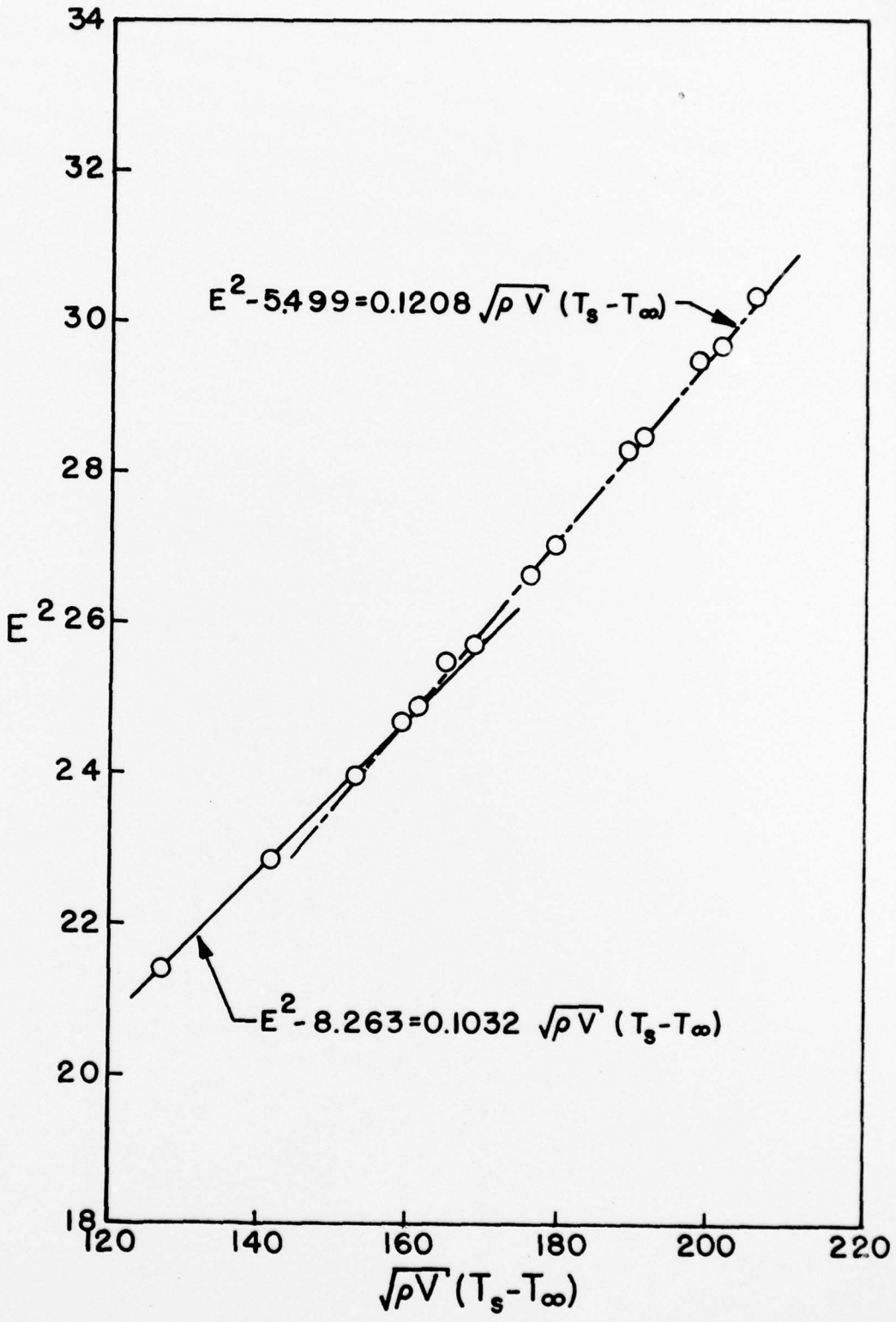

Figure 6. Results of Normal Velocity Calibration for Sensor 1.

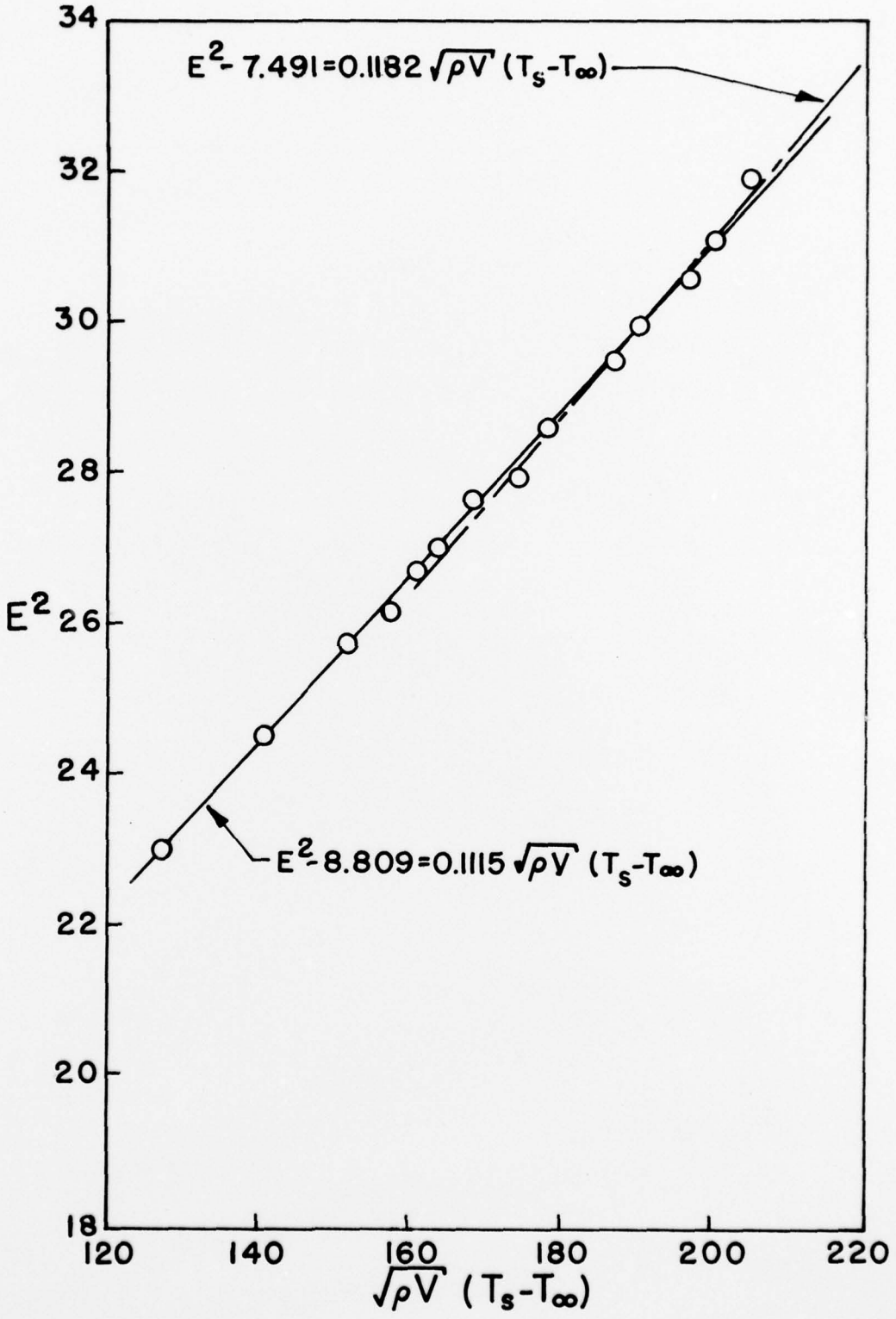

Figure 7. Results of Normal Velocity Calibration for Sensor 2.

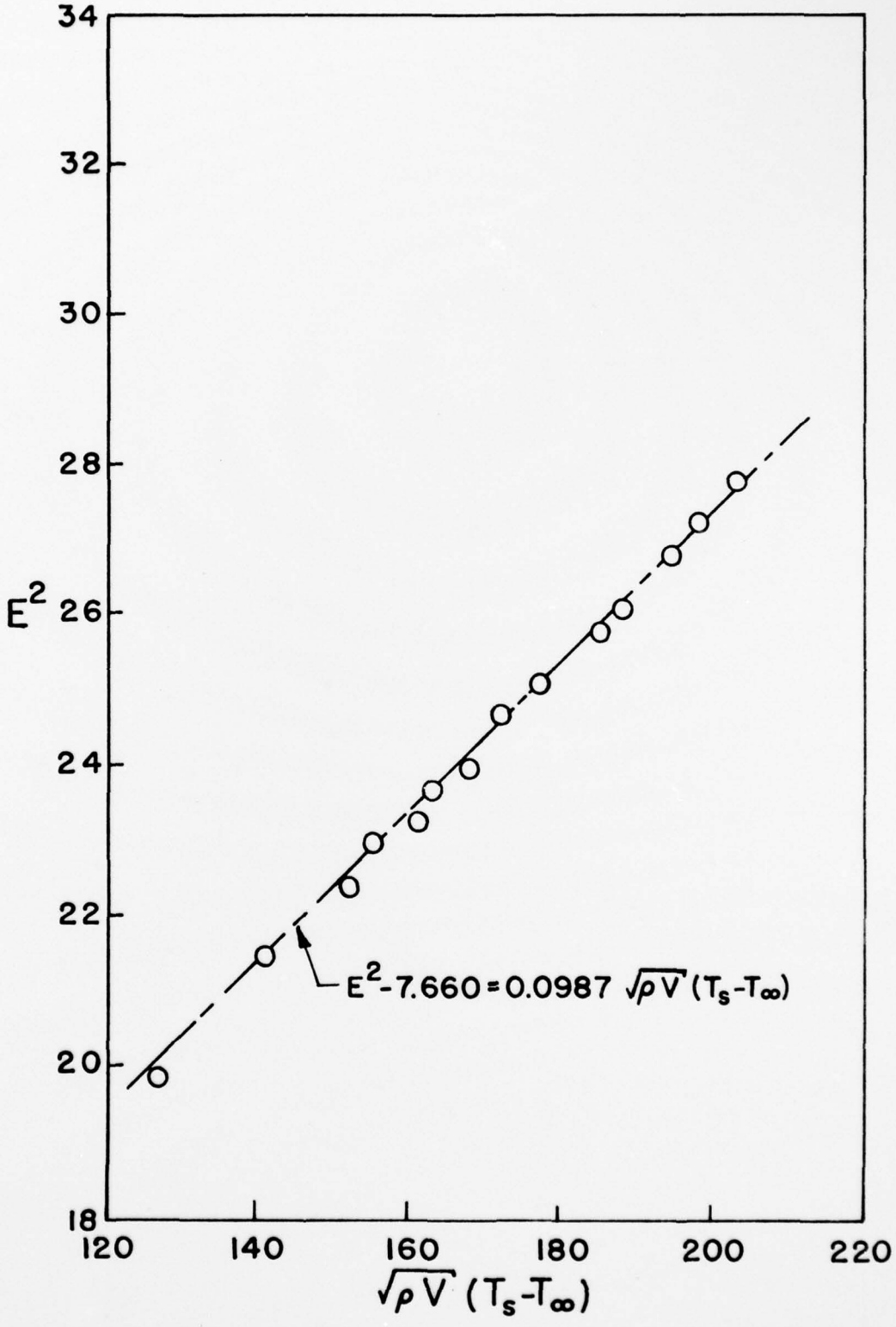

Figure 8. Results of Normal Velocity Calibration for Sensor 3.

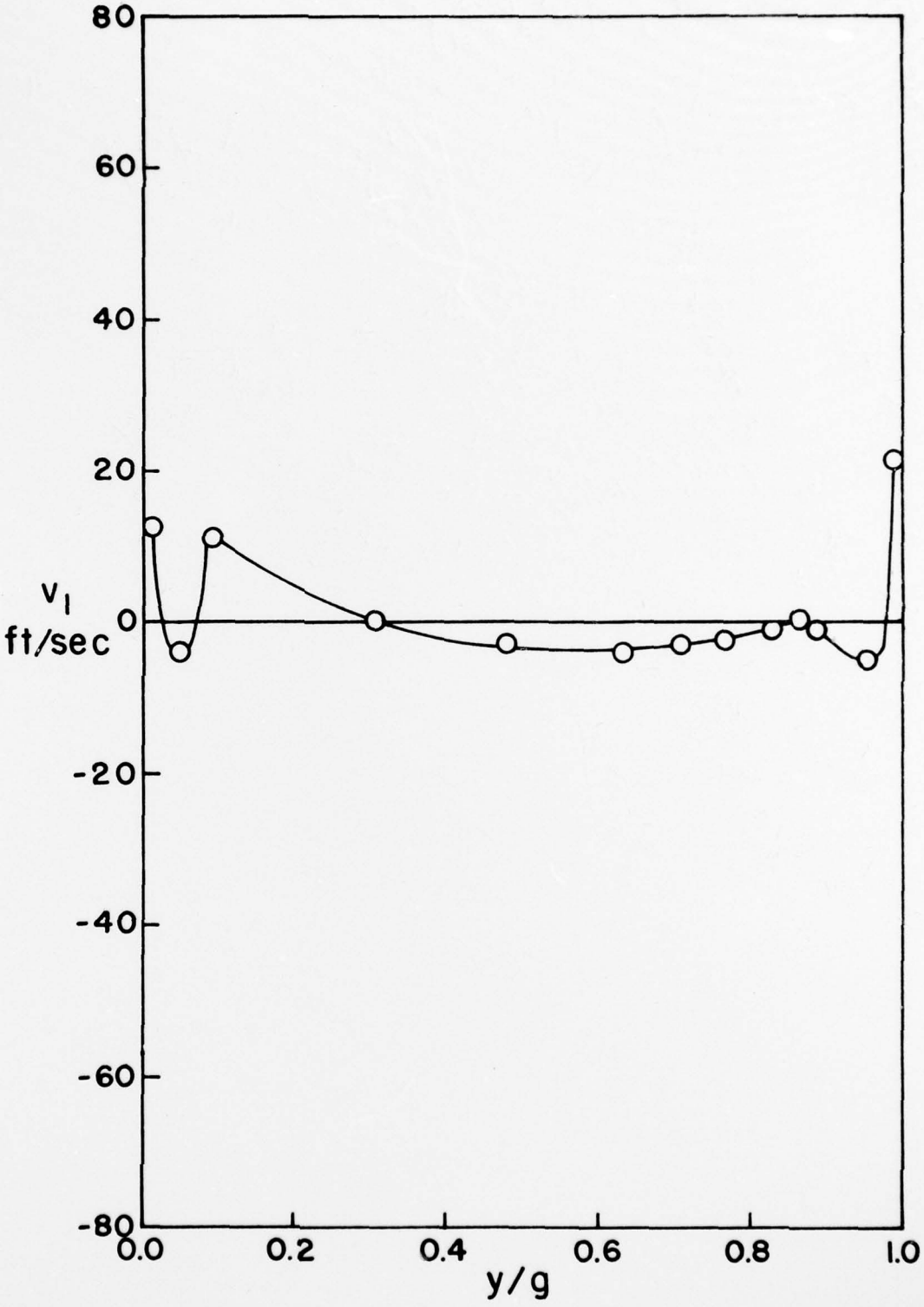

Figure 9. Radial Velocity (v_1) as a Function of Gapwise Position.

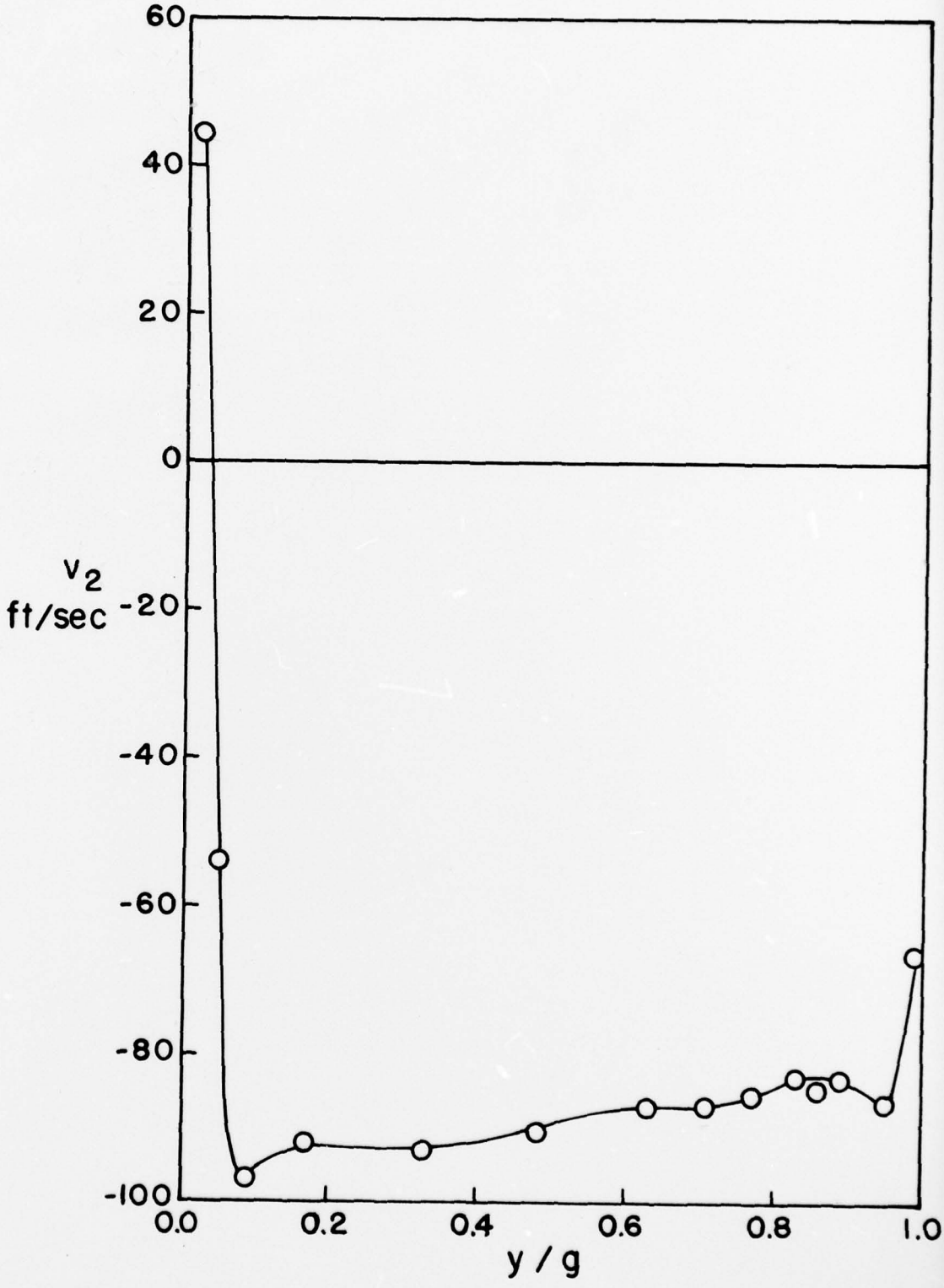

Figure 10. Circumferential Velocity (v_2) as a Function of Gapwise Position.

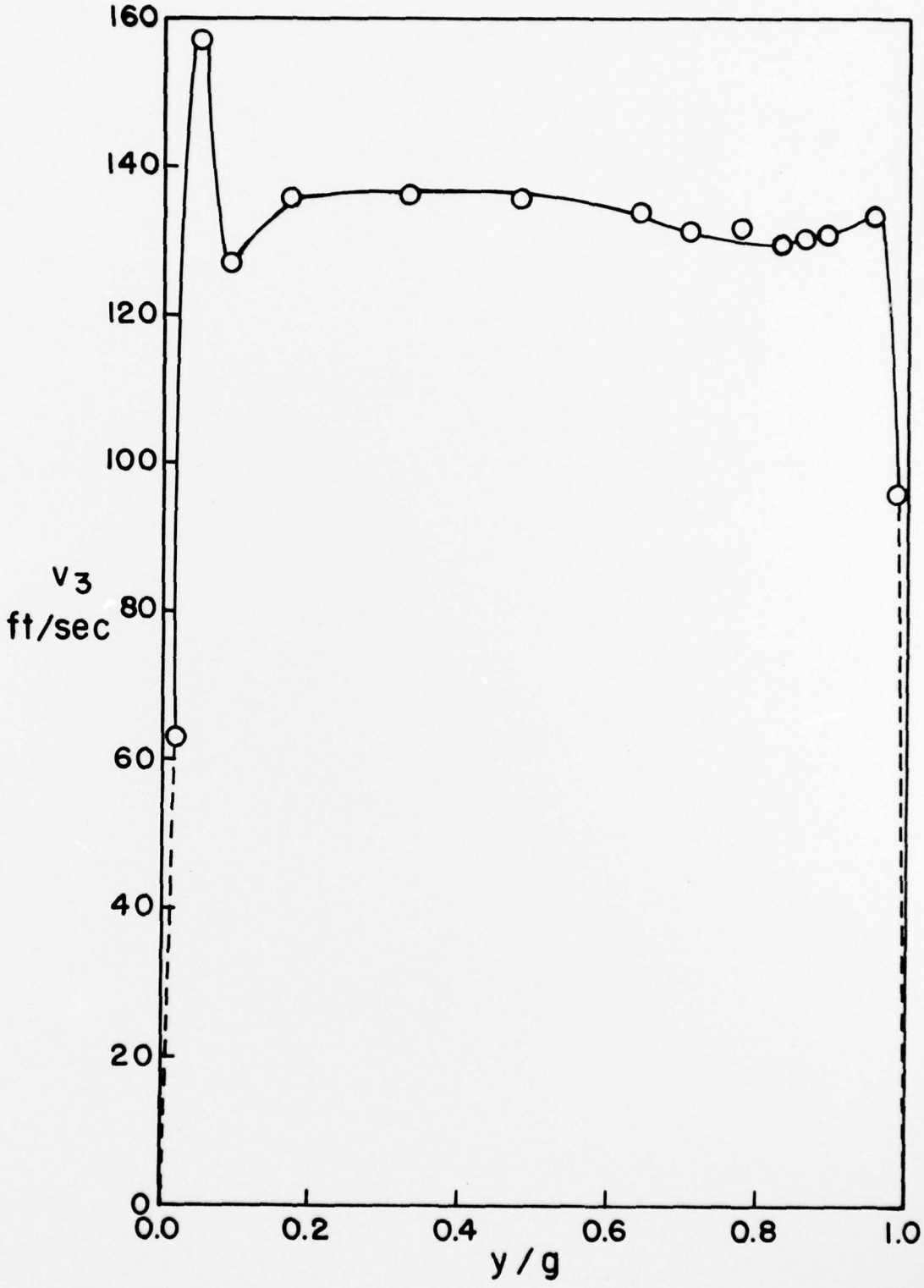

Figure 11. Axial Velocity (v_3) as a Function of Gapwise Position.

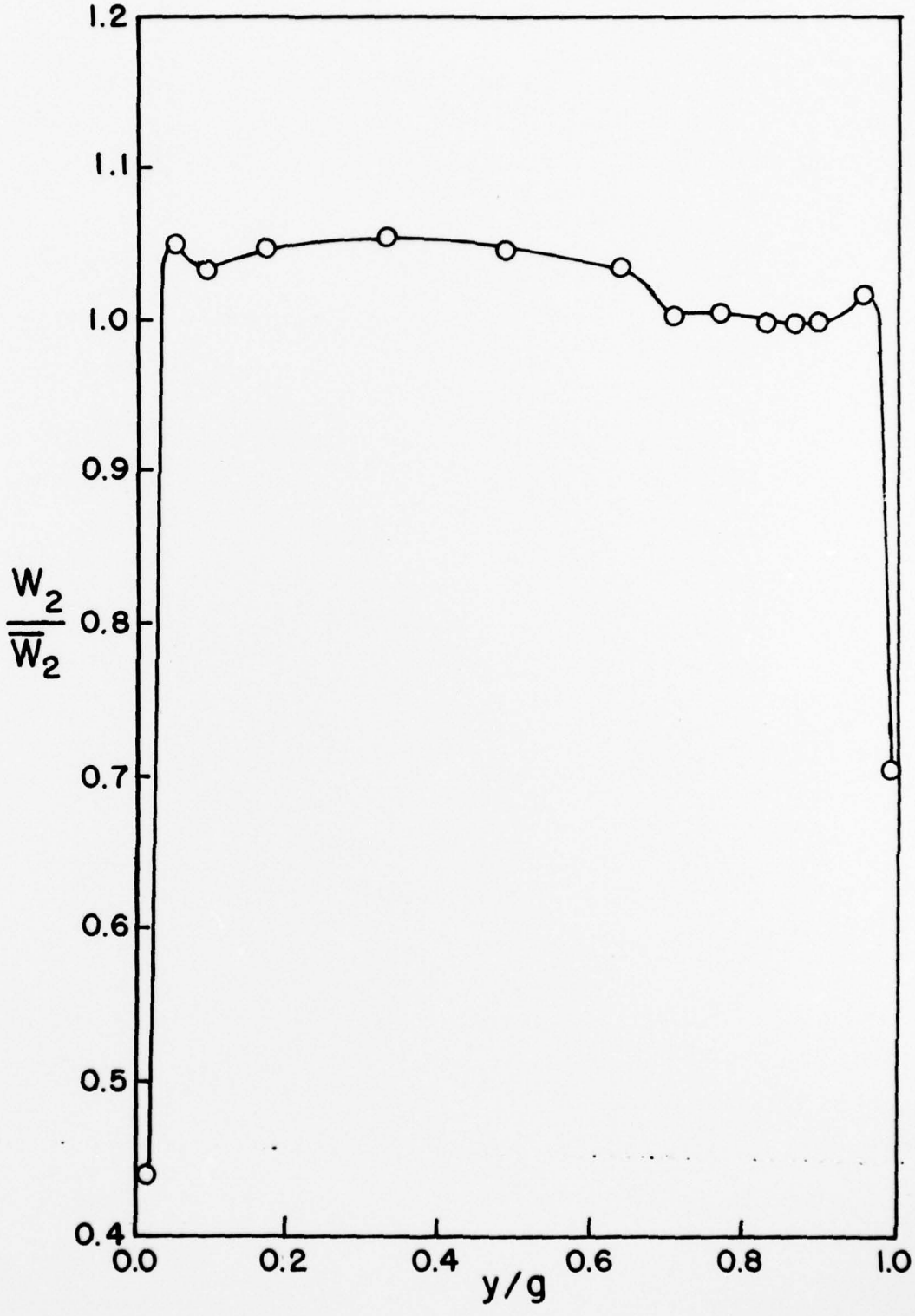

Figure 12. Normalized Velocity at Rotor Exit Plane as a Function of Gapwise Position.

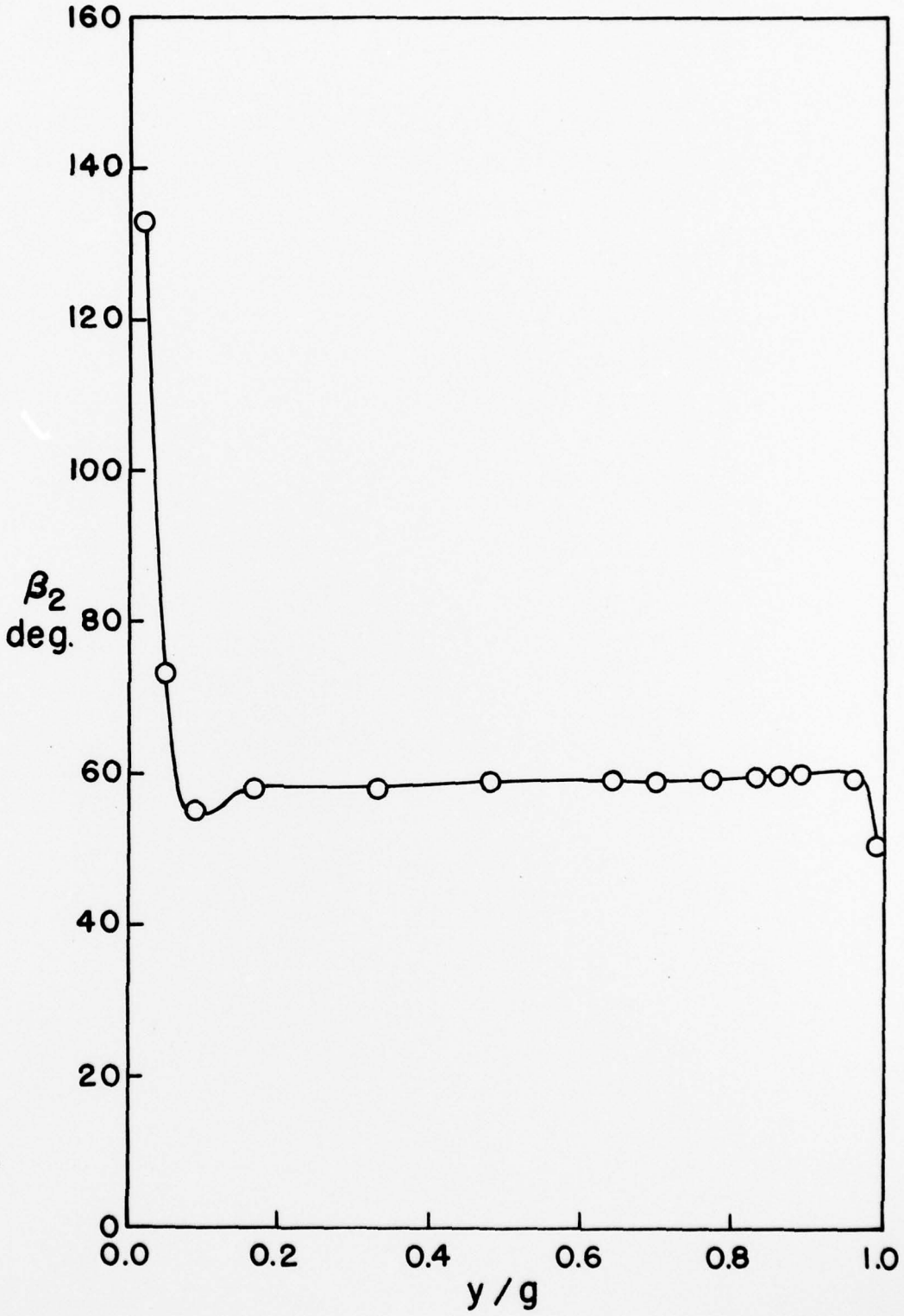

Figure 13. Circumferential Exit Angle as a Function of Gapwise Position.

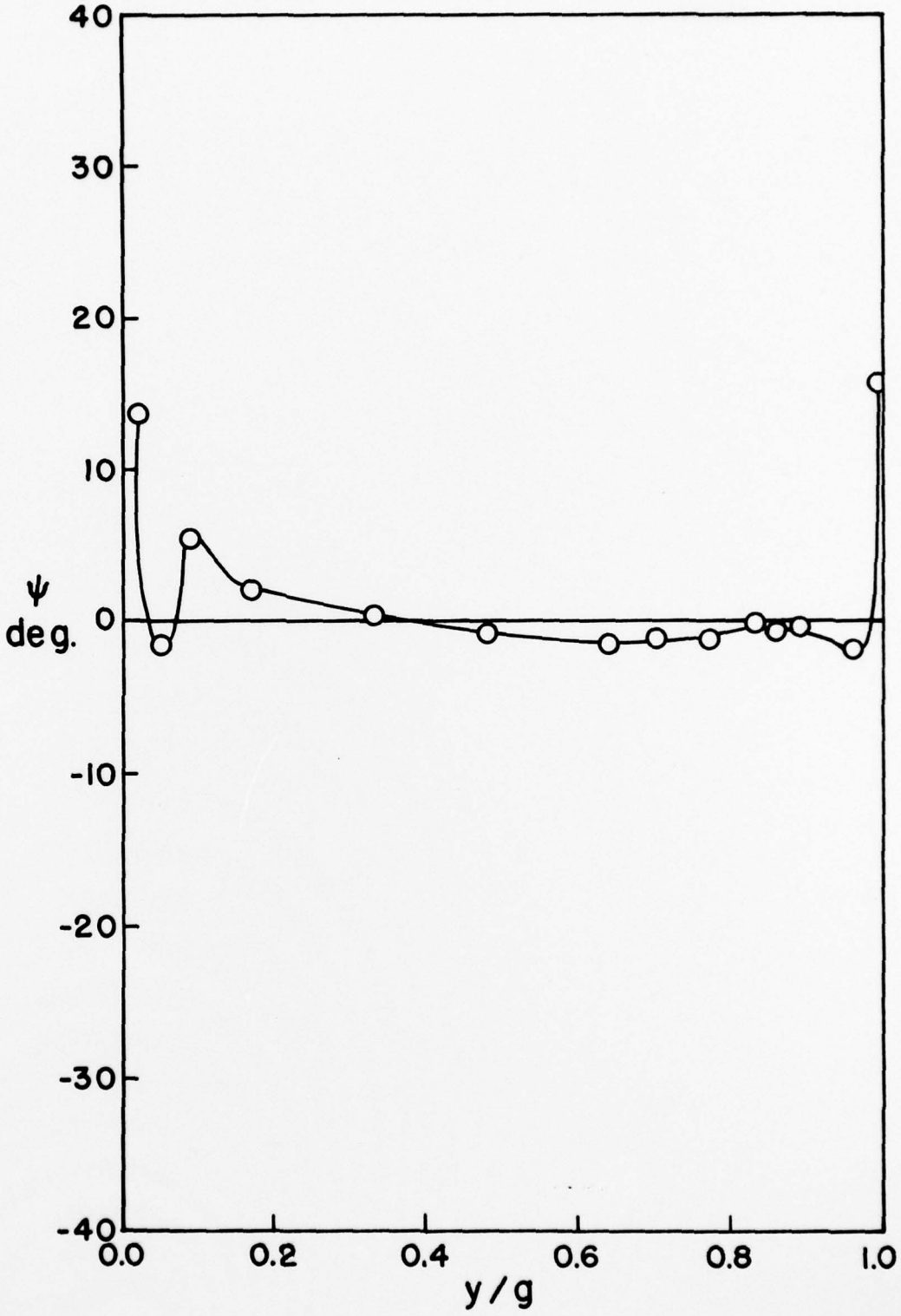

Figure 14. Radial Exit Angle as a Function of Gapwise Position.

REPORT DOCUMENTATION PAGE		READ INSTRUCTIONS BEFORE COMPLETING FORM
1. REPORT NUMBER AFOSR-TR- 78-1362	2. GOVT ACCESSION NO.	3. RECIPIENT'S CATALOG NUMBER
4. TITLE (and Subtitle) Calibration Procedures Developed for a Triaxial Hot-Film Probe and Preliminary Measurements of the Velocity Profile in the Wake of an Isolated Rotor		5. TYPE OF REPORT & PERIOD COVERED INTERIM
		6. PERFORMING ORG. REPORT NUMBER NCSU/EDC-78-4
7. AUTHOR(s) L.W. Hardin W. H. Hall		8. CONTRACT OR GRANT NUMBER(s) F44620-76-C-0055
9. PERFORMING ORGANIZATION NAME AND ADDRESS North Carolina State University School of Engineering, Engineering Design Center, Raleigh, N. C. 27650		10. PROGRAM ELEMENT, PROJECT, TASK AREA & WORK UNIT NUMBERS 2307A4 61102F
11. CONTROLLING OFFICE NAME AND ADDRESS Air Force Office of Scientific Research/NA Bldg. 410 Bolling Air Force Base, D.C. 20332		12. REPORT DATE May, 1978
		13. NUMBER OF PAGES 45
14. MONITORING AGENCY NAME & ADDRESS(if different from Controlling Office)		15. SECURITY CLASS. (of this report) Unclassified
		15a. DECLASSIFICATION/DOWNGRADING SCHEDULE

16. DISTRIBUTION STATEMENT (of this Report)
Approved for public release; distribution unlimited.

17. DISTRIBUTION STATEMENT (of the abstract entered in Block 20, if different from Report)

18. SUPPLEMENTARY NOTES

19. KEY WORDS (Continue on reverse side if necessary and identify by block number)
DYNAMIC STALL
DISTORTED FLOW
UNSTEADY FLOW
UNSTEADY BOUNDARY LAYER
TURBOCOMPRESSOR

20. ABSTRACT (Continue on reverse side if necessary and identify by block number)
In an experiment which was conducted to determine the response of an isolated rotor to an inlet distortion, a triaxial hot-film probe was used to make velocity and flow angle measurements near the exit plane of the rotor. The velocity sensors were three mutually orthogonal film-type sensors operated in the constant temperature mode. This probe has been calibrated and procedures have been developed to extract velocity components from the anemometer output voltages. It has been determined that the proximity of the probe shaft results

in severe distortion of the flow over the velocity sensors. The process which has been developed for computing velocities yields satisfactory results in test cases and is expected to be suitable for reducing the data from limited number of flow conditions for which the probe was used in the present experiment. However, it is considered to be too involved and too susceptible to error to be used in experiments where there is either a vast amount of data to be processed or there is no means of spot-checking the results. It is therefore considered mandatory that an improved probe geometry be devised which does not exhibit the degree of interference observed with the probe in question before undertaking to make extensive wake measurements.